Preprint
UCRL-JC-138490

Initial Performance of the Keck AO Wavefront Controller System

E.M. Johansson, et al

This article was submitted to The International Society for Optical Engineering International Symposium on Astronomical Telescopes and Instrumentation 2000, Munich, Germany, March 27-31, 2000

March 1, 2001

Initial performance of the Keck AO wavefront controller system

Erik M. Johansson[a], D. Scott Acton[b], Jong R. An[a], Kenneth Avicola[a], Barton V. Beeman[a], James M. Brase[a], Carmen J. Carrano[a], John Gathright[b], Donald T. Gavel[a], Randall L. Hurd[a], Olivier Lai[c], William Lupton[b], Bruce A. Macintosh[a], Claire E. Max[a], Scot S. Olivier[a], J. Christopher Shelton[d], Paul J. Stomski[b], Kevin Tsubota[b], Kenneth E. Waltjen[a], James A. Watson[a], Peter L. Wizinowich[b]

[a]Lawrence Livermore National Laboratory, Livermore, CA
[b]W. M. Keck Observatory, Kamuela, HI
[c]Canada-France-Hawaii Telescope, Kamuela, HI
[d]Carpe Photon, Paauilo, HI

ABSTRACT

The wavefront controller for the Keck Observatory AO system consists of two separate real-time control loops: a tip-tilt control loop to remove tilt from the incoming wavefront, and a deformable mirror control loop to remove higher-order aberrations. In this paper, we describe these control loops and analyze their performance using diagnostic data acquired during the integration and testing of the AO system on the telescope. Disturbance rejection curves for the controllers are calculated from the experimental data and compared to theory. The residual wavefront errors due to control loop bandwidth are also calculated from the data, and possible improvements to the controller performance are discussed.

1. INTRODUCTION

This paper describes the Keck Observatory AO system wavefront controller (WFC) and presents initial performance results derived from diagnostic data acquired during the integration and testing of the AO system on the telescope. The WFC was designed and built by personnel from Lawrence Livermore National Laboratory (LLNL) during 1996 through 1998. It was shipped to the W. M. Keck Observatory (WMKO) in late 1998 and integrated into the AO system on the Mauna Kea summit

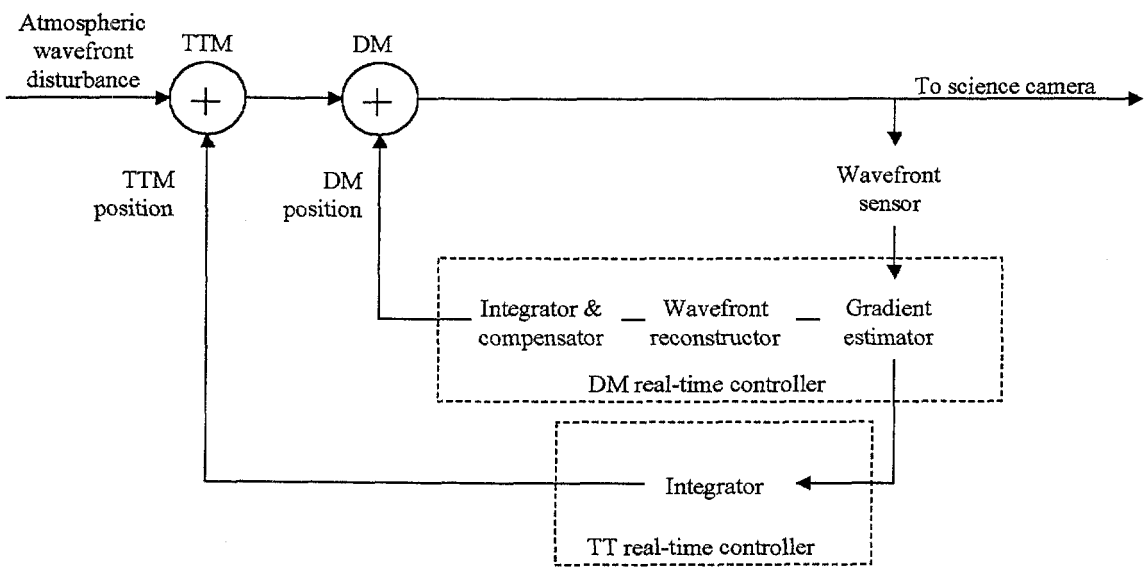

Figure 1. A block diagram of the Keck AO wavefront controller showing the two nested control loops: a deformable mirror (DM) controller and a tip-tilt (TT) controller.

by WMKO personnel in February 1999. First light for the AO system occurred on February 5, 1999. Completion of the integration and test of the WFC was conducted jointly by LLNL and WMKO during most of 1999. The AO system was officially commissioned as a facility instrument in August 1999 and is now producing high-resolution astronomical images [1,2].

The WFC consists of two separate real-time control loops: a tip-tilt controller to remove tilt from the incoming wavefront [3], and a deformable mirror controller to remove higher-order aberrations [4]. A block diagram of the two nested control loops is shown in Figure 1. We present disturbance rejection curves for each of the controllers that detail their abilities to reject atmospheric wavefront disturbances. These curves are then compared to model disturbance rejection curves based on timing measurements of delay times in the real-time control loops. We determine the unity-gain crossover frequency and derive the residual closed-loop bandwidth error for each controller. Finally, we discuss future work and possible upgrades to the controllers to improve performance.

2. THE TIP-TILT CONTROLLER

The tip-tilt controller is a simple proportional-integral (PI) controller that receives an estimate of the average wavefront tilt from the deformable mirror controller, applies the loop gain, integrates, and finally computes a new tip-tilt mirror position vector. The controller is discussed in detail in reference [3]. A sample disturbance rejection curve for the tip-tilt controller is shown in Figure 2. The disturbance rejection curve is a measure of how the controller rejects atmospheric wavefront disturbances in closed-loop mode relative to open-loop mode (no rejection). It is calculated by dividing estimates of the closed-loop and open-loop wavefront tilt power spectra (see Figure 3). The power spectral estimates were obtained by averaging individual power spectra from tip-tilt diagnostics data over an ensemble of 10 data sets.

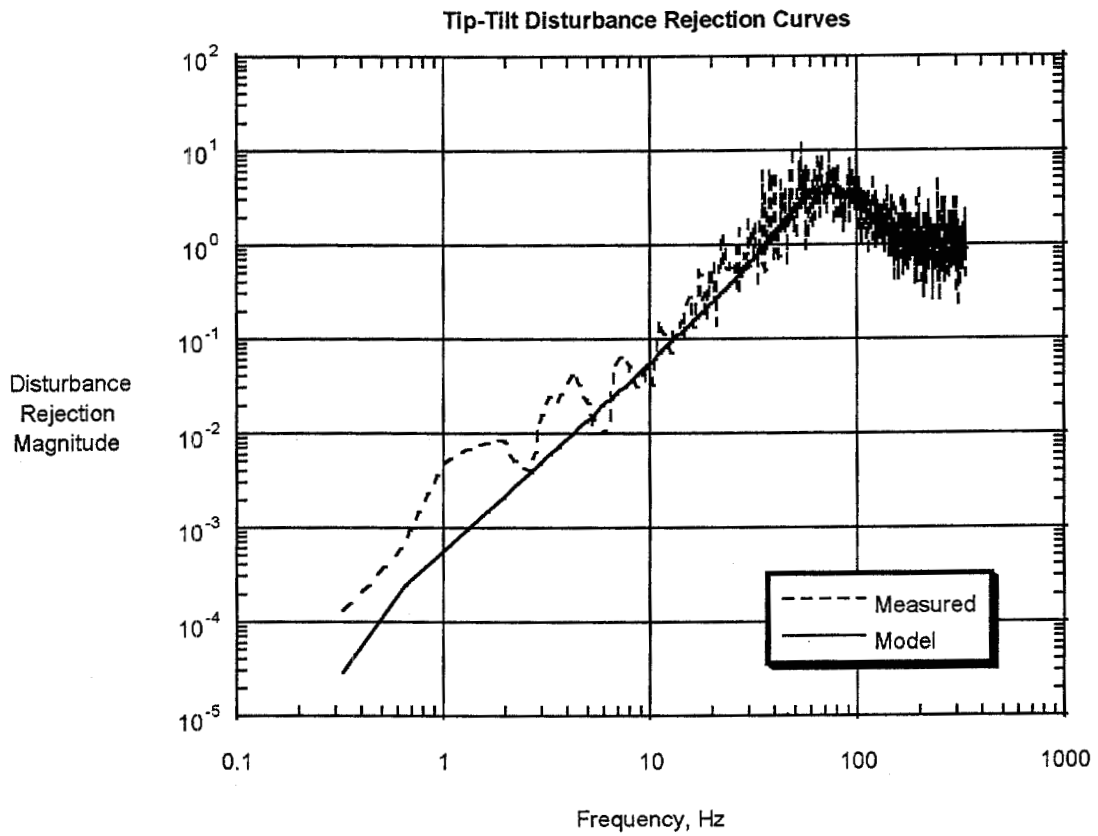

Figure 2. Disturbance rejection curves for the tip-tilt controller. The unity-gain crossover frequency is 33 Hz for a loop gain of 0.4

A model disturbance rejection curve for the controller is also shown in the figure. The details of the model are discussed below in Section 5. The excellent agreement between the experimental data and the model indicates that the controller is performing as expected. From the model curve, we are able to determine the unity-gain crossover frequency, which is 33 Hz in this case. This is the frequency where the disturbance rejection curve crosses the value 1. At this frequency the controller is no longer able to reject the tip-tilt disturbance due to the atmosphere, and actually begins to amplify disturbances. Thus, this frequency represents the disturbance rejection bandwidth of the tip-tilt controller.

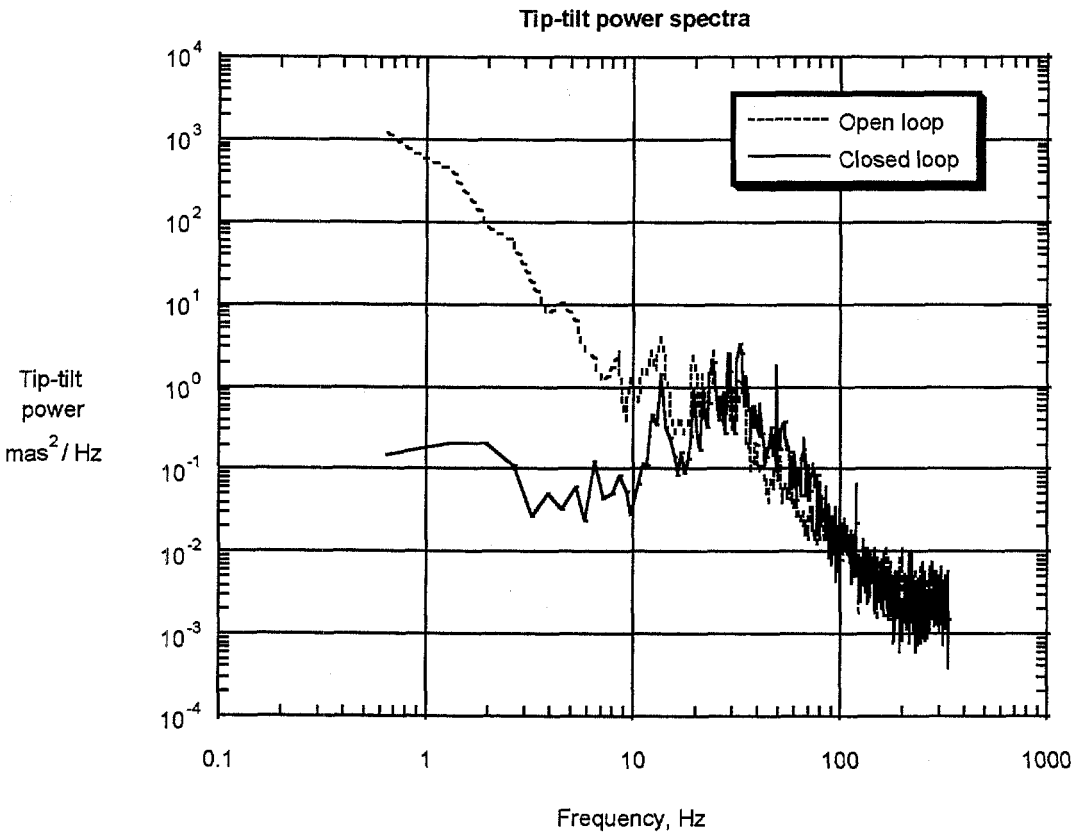

Figure 3. Open-loop and closed-loop tip-tilt power spectra. The residual bandwidth error of the controller is determined by subtracting the noise floor from the closed-loop power spectrum and integrating. For this data set, the residual tip-tilt bandwidth error is found to be 5.6 milli-arc-seconds rms.

The residual controller bandwidth error may be computed by subtracting the noise floor (the asymptotic value at high frequencies) from the closed-loop tip-tilt power spectrum and integrating. This is illustrated in Figure 3, which shows open-loop and closed-loop wavefront tilt power spectra for the tip-tilt controller. The difference between the upper and lower curves represents the atmospheric tip-tilt disturbance which is rejected (or eliminated) by the controller. The lower curve represents residual tip-tilt error, which, after subtracting the noise floor and integrating, results in the residual bandwidth error of the controller. For the data set shown in Figure 3, the residual controller bandwidth error is found to be 5.6 milli-arc-seconds rms.

3. THE DEFORMABLE MIRROR CONTROLLER

The deformable mirror controller is a PI controller with compensation for the loop time delay. It is discussed in detail in reference [4]. The controller initially receives raw CCD image data from the wavefront sensor (a Hartmann sensor using an Adaptive Optics Associates camera with a MIT Lincoln Lab CCD) and computes centroids for each of the subapertures using a quad-cell calculation to estimate the wavefront gradient. Next, the controller performs a matrix-vector multiply to compute

the new mirror position vector and applies the loop gain, integration, and compensation. Finally, the new mirror position vector is sent to the high voltage amplifiers that drive the deformable mirror to its new position.

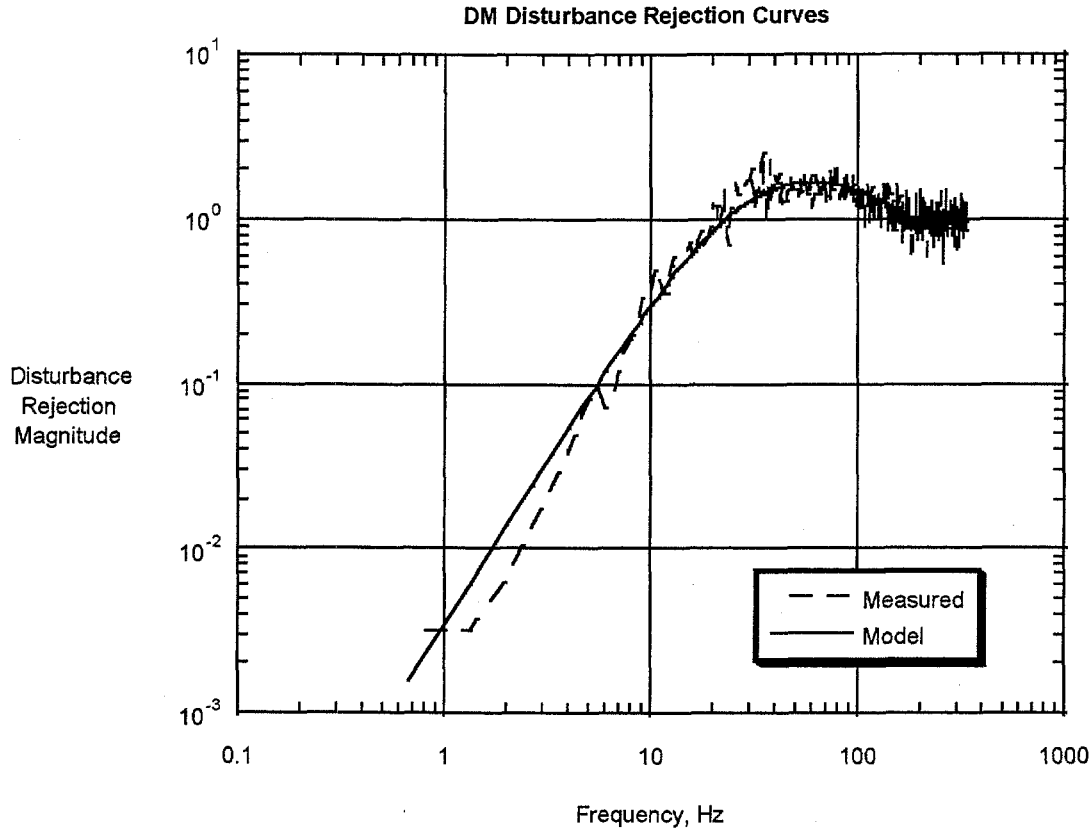

Figure 4. Disturbance rejection curves for the deformable mirror controller. The unity-gain crossover frequency is 23 Hz for a loop gain of 0.5

A sample disturbance rejection curve is shown in Figure 4. The disturbance rejection curve is calculated in a manner similar to that described above for the tip-tilt controller using diagnostics data from the deformable mirror controller (see Figure 5). In this case, however, the average power spectra used to derive the disturbance rejection curve are computed by averaging the wavefront phase power spectrum for each deformable mirror actuator over all the actuators and then averaging over 10 data sets. A model disturbance rejection curve for the controller is also shown in the figure. The details of the model are discussed below in Section 5. Again, the excellent agreement between the experimental data and the model indicates that the controller is performing as expected. From the model curve we determine that the unity-gain crossover frequency is 23 Hz under these conditions. Note that the crossover frequency is somewhat low due to the low controller loop gain used in this particular data set, 0.5. A higher loop gain would result in an increase in the crossover frequency. Using a loop gain of 0.8, we have measured crossover bandwidths of 30 Hz, in accordance with the model prediction.

The residual controller bandwidth error may be computed by subtracting the noise floor from the closed-loop wavefront phase power spectrum and integrating, similar to what was done for the tip-tilt controller. This is illustrated in Figure 5, which shows open-loop and closed-loop wavefront phase power spectra for the deformable mirror controller. The difference between the upper and lower curves represents the atmospheric wavefront phase disturbance which is rejected by the controller. The lower curve represents residual wavefront phase error, which, after subtracting the noise floor and integrating, results in the residual bandwidth error of the controller. For the data set shown in Figure 5, the residual controller bandwidth error is found to be 117 nm rms.

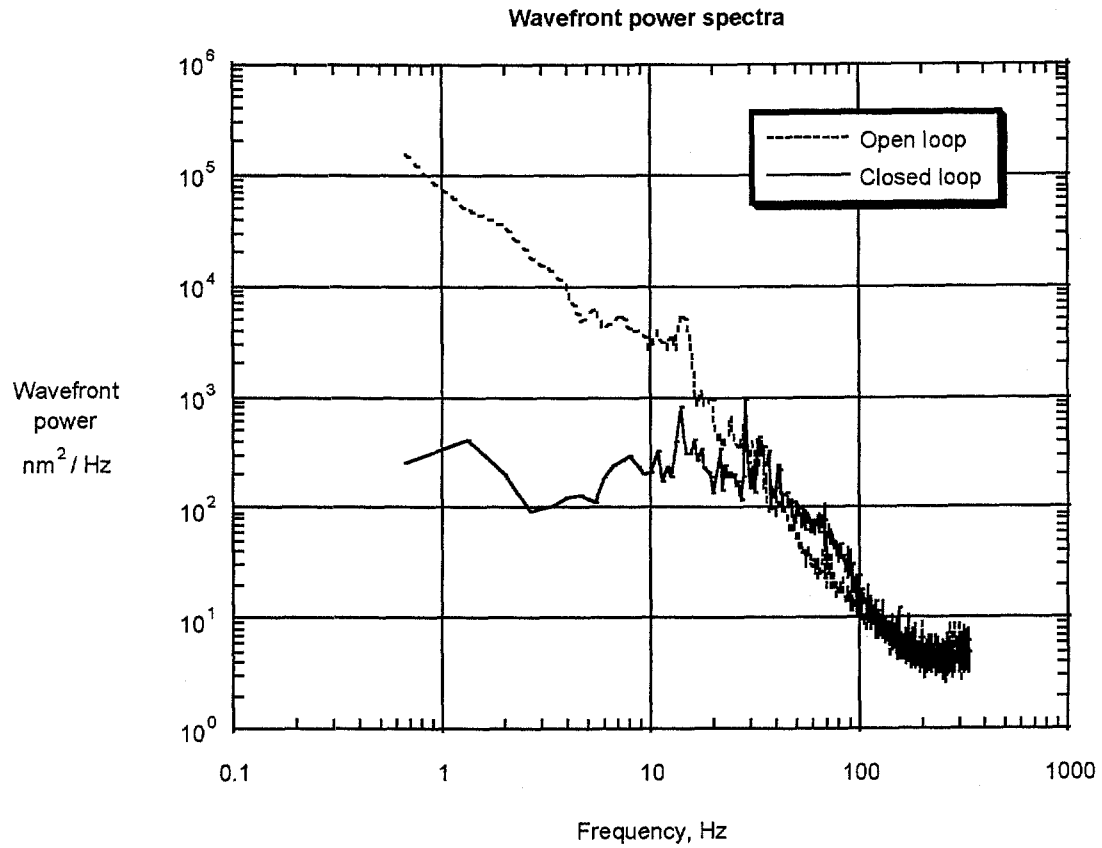

Figure 5. Open-loop and closed-loop wavefront phase power spectra. The residual bandwidth error of the controller is determined by subtracting the noise floor from the closed-loop power spectrum and integrating. For this data set, the residual wavefront phase bandwidth error is found to be 117 nm rms.

4. ERROR BUDGET

An error budget is fundamental to understanding the performance of the Keck AO system. An error budget details the various sources and amounts of error present in the system and serves as a tool to predict the theoretical system performance. The initial Keck AO system error budget was constructed during the system design phase of the project. We are now beginning to replace the various estimated values in the error budget with values derived from AO system performance diagnostics data. The error budget updated with the two controller bandwidth error terms computed above is shown in Figure 6. The measured deformable mirror and tip-tilt controller bandwidth errors are comparable to the predicted errors from deformable mirror fitting and uncorrectable telescope primary mirror errors. These four terms account for the majority of the expected residual error.

5. SYSTEM MODELING

The model disturbance rejection curves used above were generated using Mathematica and standard signal processing models for the various components in each controller. Coefficients and constants in the models are all based on either the design of the controller or the parameters used to record the diagnostic data (loop rate, loop gain). Each controller model contains the following components: wavefront sensor, zero-order-hold, compute delay, and integrator/compensator. The wavefront sensor

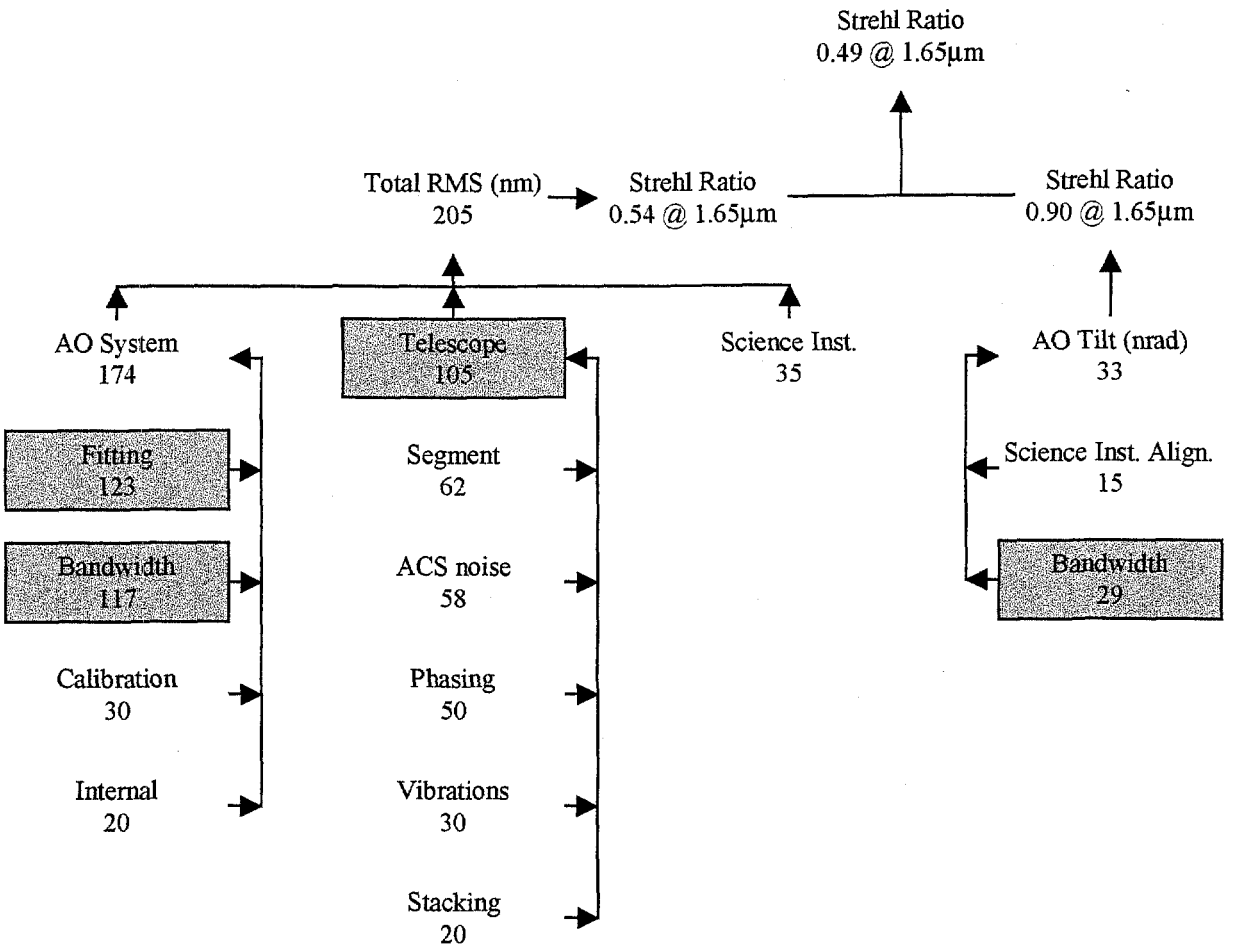

Figure 6. The Keck Natural Guide Star AO system error budget, assuming a bright guide star, everything on axis, and median seeing conditions at a 30 degree zenith angle. The numbers have been updated to include bandwidth errors for the tip-tilt and deformable mirror controllers derived from controller diagnostics data, as described above.

and zero-order-hold models are the same for each controller, whereas the compute delay and integrator/compensator models are different. For each controller, the integration and sampling done by the wavefront sensor camera is modeled as an integrator with a delay, which has the following transfer function:

$$H_{Cam}(s) = \frac{1 - e^{-sT}}{sT} \tag{1}$$

where T represents the sample time (the reciprocal of the loop rate) and s is the complex frequency variable. For the examples discussed in this paper, the loop rate is 670 Hz; hence, T is 1.493 ms. The sampled data produced by the wavefront sensor is held constant by the real-time codes during the remainder of a loop cycle; therefore, a zero-order-hold model must be used to represent this. Coincidentally, the zero-order-hold has the same transfer function as the integrator and delay described above for the camera:

$$H_{ZOH}(s) = \frac{1 - e^{-sT}}{sT} \tag{2}$$

The compute delay in the controllers is modeled as a simple delay:

$$H_{delay}(s) = e^{-s\tau_c} \tag{3}$$

where τ_c is the compute delay time of the controller (described below). The integrators and compensators used are discussed separately below for each controller.

For the tip-tilt controller, the total delay time from wavefront acquisition to mirror movement has been estimated to be 1.65 ms. The delay time was computed by adding the delay time of the wavefront gradient estimator to the compute delay of the tip-tilt controller. The delay time of the gradient estimator represents the time from wavefront acquisition until the wavefront gradient estimate is received by the tip-tilt controller. The compute delay of the tip-tilt controller was measured using timestamps in the real-time code, averaging over a sufficient number of loop iterations to minimize error. Additional parameters used in the model are the loop gain, which was 0.4, and a fixed-gain scaling constant in the real time code, which is 0.8. The tip-tilt controller uses a single integrator without compensation, which, when combined with the fixed-gain and loop gain constants described above, has a discrete-time transfer function of:

$$H_{TT}(z) = \frac{(0.4)(0.8)z}{z - 1} \tag{4}$$

where z is the complex Z-transform variable. For the deformable mirror controller, the total delay time has been estimated to be 2.13 ms. As in the case of the tip-tilt controller, the delay time was measured using timestamps in the real-time code and averaging over a sufficient number of loop iterations to minimize error. Additional parameters used in the model are the loop gain, which was 0.5, and a compensator weight, which is 0.25. The deformable mirror controller uses an integrator with compensation, which, when combined with these parameters, has a discrete-time transfer function of:

$$H_{DM}(z) = \frac{0.5z^2}{(z-1)(z-0.25)} \tag{5}$$

All of the above model components are combined using Mathematica to generate the model disturbance rejection curves for each controller over the frequencies of interest.

6. CONCLUSION

We have presented initial performance results for the wavefront controller in the Keck AO system. The disturbance rejection curves for both the tip-tilt and deformable mirror controllers agree closely with model curves based on control loop timing measurements. We have derived the unity-gain crossover frequencies for each controller as well as the residual bandwidth errors. Future work includes measurement of the other error budget terms and comparison of Strehl ratios predicted by measured error budget terms with measured image Strehl ratios. Based on the results of this analysis, system upgrades to improve performance will be considered. Furthermore, we plan to increase the tip-tilt controller bandwidth by using a very fast avalanche photo diode tilt sensor that will run independently of the Hartmann sensor used for wavefront gradient estimation. A possible upgrade to faster processors in the deformable mirror controller is also being considered.

7. ACKNOWLEDGEMENTS

This work was performed under the auspices of the U.S. Department of Energy by University of California Lawrence Livermore National Laboratory under contract No. W-7405-Eng-48. The W. M. Keck Foundation provided funding for the AO facility, with additional funding from NASA and LLNL.

8. REFERENCES

1. P. Wizinowich, D. S. Acton, C. Shelton, P. Stomski, J. Gathright, K. Ho, W. Lupton, K. Tsubota, O. Lai, C. Max, J. Brase, J. An, K. Avicola, S. Olivier, D. Gavel, B. Macintosh, A. Ghez, and J. Larkin , "First Light Adaptive Optics Images from the Keck II Telescope: A New Era of High Angular Resolution Imagery", Publications of the Astronomical Society of the Pacific VOLUME 112, NUMBER 769, MARCH 2000, pages 315-319.

2. "Getting a Clear View", Science News, Vol. 157, No. 10, March 4, 2000, p. 156.

3. K. Avicola, J. Watson, B. Beeman, T. Kuklo, and J. Taylor, "Design and performance of the tip-tilt subsystem for the Keck II telescope adaptive optics system," *in Adaptive Optical System Technologies*, Domenico Bonacinni, Robert K. Tyson, Editors, Proceedings of SPIE Vol. 3353, 628-637 (1998).

4. J. M. Brase, J. An, K. Avicola, B. V. Beeman, D. T. Gavel, R. Hurd, B. Johnston, H. Jones, T. Kuklo, C. E. Max, S. S. Olivier, K. E. Waltjen, and J. Watson, "The wavefront control system for the Keck Telescope," *in Adaptive Optical System Technologies*, Domenico Bonacinni, Robert K. Tyson, Editors, Proceedings of SPIE Vol. 3353, 517-521 (1998).